Journal of Materials Chemistry C

PAPER

View Article Online
View Journal | View Issue

Cite this: J. Mater. Chem. C, 2019, 7, 11220

Mn^{2+}-Based narrow-band green-emitting Cs_3MnBr_5 phosphor and the performance optimization by Zn^{2+} alloying†

Binbin Su,[a] Maxim S. Molokeev[bcd] and Zhiguo Xia *[a]

Received 29th July 2019,
Accepted 17th August 2019

DOI: 10.1039/c9tc04127c

rsc.li/materials-c

To discover new narrow-band green-emitting phosphors is a challenge for backlighting light-emitting diodes (LEDs) used in liquid crystal displays (LCDs). The synthesis and optical properties of Cs_3MnBr_5 are demonstrated herein. The intrinsic Mn^{2+} luminescence without concentration quenching leads to intense green emission at 520 nm with narrow full width at half maximum of 42 nm and high photoluminescence quantum yield (PLQY) of 49% under the excitation at 460 nm. When a small amount of Zn^{2+} is introduced into Cs_3MnBr_5, the luminescence intensity decreases slightly. However, the thermal stability of Cs_3MnBr_5 is improved from 82% to 87% with the intensity values at 423 K compared to that at 298 K. The white LED device fabricated using $Cs_3Mn_{0.96}Zn_{0.04}Br_5$ (green) and $K_2SiF_6:Mn^{4+}$ (red) phosphors with a blue LED chip exhibit a high luminous efficiency (107.76 lm W^{-1}) and wide color gamut (101% National Television System Committee standard (NTSC) in Commission Internationale de L'Eclairage (CIE) 1931 color space), demonstrating its potential application in wide color gamut LCD backlights.

1. Introduction

Phosphor-converted light-emitting diodes (LEDs) based on a blue-emitting InGaN chip act as a new backlight technology, which has been widely used in modern liquid crystal displays (LCDs) owing to its spectral adjustability, stability and high light efficiency.[1–3] In this technique, the luminescence properties of green and red emitters, such as peak position and full-width at half-maximum (FWHM) significantly affect the gamut range, color purity, luminescence efficiency and reliability of backlight units.[4,5] Therefore, it is crucial to develop narrow-band green or red phosphors in a suitable spectral region to enlarge the maximum accessible color gamut and color purity, and increase the visual luminous efficacy for extending the practical applications. Since the human eyes are able to clearly distinguish green light, the discovery of highly efficient narrow-band green-emitting phosphors seems to be particularly important and acts as the main topic herein. In the typical commercial wide gamut LED backlight devices, the narrow-band green-emitting phosphor, β-SiAlON:Eu^{2+}, with the emission peaking at 540 nm is considered as the optimum choice.[6] Although the luminescence properties of β-SiAlON:Eu^{2+} is significantly high, the unsatisfied FWHM limits the maximum accessible color gamut for backlighting display application (90% of NTSC).[7]

Recently, various narrow-band green-emitting materials have been developed including three main categories, namely, perovskite quantum dots (PQDs),[8,9] rare earth doped phosphors[10–13] and Mn^{2+} activated phosphors.[14–18] The $CsPbBr_3$ PQDs emerged as the green phosphors for wide-color gamut backlight display due to their high photoluminescence quantum yield (PLQY) and superior narrow emission bands with an FWHM of only ≈20 nm. The white LED fabricated with green-emitting $CsPbBr_3$/SDDA@PMMA, red phosphor KSF:Mn^{4+} and blue LED chip, exhibits high color-gamut with 102% of NTSC. However, the unstable PLQY caused by poor stability and the degradation behavior in ambient environment are the achilles heel, restricting their commercial applications.[8,19,20] On the contrary, inorganic green phosphors beyond β-SiAlON:Eu^{2+} also exhibit high luminescence efficiency, moisture resistance and excellent thermal stability in this application. Xie *et al.* reported $Ba_2LiSi_7AlN_{12}:Eu^{2+}$ and $Ba[Li_2(Al_2Si_2)N_6]:Eu^{2+}$ green phosphors with emissions peaking at ≈515 nm and 532 nm with an FWHM of 61 nm and 57 nm, respectively. However, they could not satisfy the maximum accessible color gamut of backlights due to the unmatched FWHM and peak position along with the harsh synthesis condition, further restricting the application.[10,11] Recently, our group discovered several novel UCr_4C_4-related narrow-band green-emitting phosphors in which $RbLi(Li_3SiO_4)_2:Eu^{2+}$

[a] State Key Laboratory of Luminescent Materials and Devices and Institute of Optical Communication Materials, South China University of Technology, Guangzhou 510641, China. E-mail: xiazg@scut.edu.cn
[b] Laboratory of Crystal Physics, Kirensky Institute of Physics, Federal Research Center KSC SB RAS, Krasnoyarsk 660036, Russia
[c] Siberian Federal University, Krasnoyarsk 660041, Russia
[d] Department of Physics, Far Eastern State Transport University, Khabarovsk 680021, Russia

† Electronic supplementary information (ESI) available. See DOI: 10.1039/c9tc04127c

showed a green emission at 530 nm with a narrow FWHM of 42 nm and an NTSC value of 107%. To further optimize the luminescence properties and improve the stability, the Na^+ was substituted for Li^+ and the green emission of $RbNa(Li_3SiO_4)_2$:Eu^{2+} was obtained with the emission peaking at 523 nm and FWHM of 41 nm. Meanwhile, the color gamut of WLED was also improved from 107% to 113% NTSC and the chemical stability has also been significantly improved. In addition to $CsPbBr_3$, perovskite QDs and rare earth Eu^{2+} doped green emitting phosphors, transition metal Mn^{2+} activated green phosphors can also have potential applications in LED backlight. For example, γ-AlON:Mn^{2+}, Mg^{2+} exhibits a FWHM of 44 nm with a color gamut of 102% NTSC and $MgAl_2O_4$:Mn^{2+} has a FWHM of 35 nm with a color gamut of 116% NTSC. Moreover, the $Sr_2MgAl_{22}O_{36}$:Mn^{2+} phosphor has a narrow FWHM of 26 nm and wide color gamut with 127% of NTSC. For $ZnAl_2O_4$:Mn^{2+}, the FWHM can be even tuned to 18 nm.[15–18] However, the emission of Mn^{2+} belongs to the spin-forbidden d–d transition from $^4T_1$ excited state to $^6A_1$; thus, Mn^{2+}-doped green phosphors generally have low absorption efficiency or quantum efficiency. Moreover, the long fluorescence lifetime compared with that of rare earth Eu^{2+}-doped phosphors will restrict the applications.

As mentioned above, perovskite QDs possess the characteristic narrow-band emission, but lack high physicochemical stability due to the existence of intrinsic defects. Inorganic phosphors normally show excellent stability, but have unsatisfactory FWHM for the emission band. Therefore, the discovery of physicochemical stability and efficient narrow-band green-emitting phosphors are urgent. Herein, we have developed a new Mn^{2+}-based narrow-band green-emitting phosphor Cs_3MnBr_5 with intrinsic Mn^{2+} emission, which can be irradiated effectively using a blue LED chip and shows a narrow band (FWHM = 42 nm) green emission peaking at 520 nm with high PLQYs (49%) and a relative short fluorescence lifetime of 0.29 ms. The luminescence intensity of Cs_3MnBr_5 is also almost retained in low Zn^{2+} doped concentrations. It is worth noting that after doping 4% Zn^{2+} into Cs_3MnBr_5, the thermal stability obviously improved from 82 to 87% with the intensity values at 423 K compared to that at 298 K. In addition, the white LED device fabricated by Cs_3MnBr_5 (green) and K_2SiF_6:Mn^{4+} (red) phosphors using a blue LED chip was obtained with high efficiency (108.88 lm W^{-1}) and wide color gamut (104% NTSC). After doping 4% Zn^{2+} into Cs_3MnBr_5, the stability of the white LED device fabricated with $Cs_3Mn_{0.96}Zn_{0.04}Br_5$ green phosphor was improved compared to those of the undoped ones, which indicates that $Cs_3Mn_{0.96}Zn_{0.04}Br_5$ has potential as green-emitting phosphors for backlighting display applications.

2. Experimental section

2.1 Materials and preparation

The polycrystalline samples of Cs_3MnBr_5 and Zn^{2+}-doped Cs_3MnBr_5 were synthesized by evaporative crystallization using stoichiometric amounts of Cs_2CO_3 (99.99%, Aladdin), $MnCO_3$ (99.95%, Aladdin), and ZnO (99.99%, Aladdin). In a typical procedure for the synthesis of Cs_3MnBr_5, 1.5 mmol Cs_2CO_3 and 1 mmol $MnCO_3$ were dissolved in a desired amount of the HBr. After the dissolution of reactants, excess acid was boiled off and the solutions were evaporated to dryness. The obtained samples were dissolved in adequate ethyl alcohol to wash away the superfluous impurity. Finally, the obtained products were dried at 373 K for 2 h in air.

2.2 Fabrication of PC-LEDs

The white LEDs were fabricated by integrating the Cs_3MnBr_5 or $Cs_3Mn_{0.96}Zn_{0.04}Br_5$ green phosphor, the KSF:Mn^{4+} commercial red phosphor (Beijing Yuji Science &Technology Co., Ltd, China) and blue LED InGaN chips (450–460 nm, 2.7–3.4 V, 300 mA, Shenzhen VANDO Technology Co., Ltd, China). The phosphors were thoroughly mixed using an epoxy resin and the obtained mixture was coated on the LED chips. The photoelectric properties, such as, the emission spectrum, color temperature (CCT), color rendering index (Ra) and CIE color coordinate of the LED were collected using an integrating sphere spectroradiometer system (ATA-1000, Ever fine).

2.3 Characterization

Structural characterization was conducted using an Aeris powder X-ray diffraction (XRD) diffractometer (PANalytical Corporation, Netherlands) operating at 40 kV and 40 mA with monochromatized Cu Kα radiation (λ = 1.5406 Å). The data used for Rietveld analysis (2θ range 10–105°) was collected in a step-scanning mode with a step size of 0.01° and 10 s counting time per step. The Rietveld structure refinements were performed by using TOPAS 4.2. The electron paramagnetic resonance (EPR) spectra were recorded by an electron paramagnetic resonance EPR spectrometer (Bruker, A300). The room-temperature photoluminescence (PL) and photoluminescence excitation (PLE) spectra were obtained on a FLS920 fluorescence spectrophotometer (Edinburgh Instruments Ltd, UK) with the Xe900 lamp as the excitation source. The same instrument was used to collect the decay data with a μF900 lamp used as the excitation source. Temperature-dependent PL spectra measurement were conducted on a fluorescence spectrophotometer (F-4600, HITACHI, Japan) and the phosphor powders were heated to 523 K with a 25 K interval at a heating rate of 100 K min^{-1} and held at each temperature for 10 min for attaining thermal equilibrium. The PLQYs were measured by a Quantaurus-QY spectrophotometer equipped with an integrating sphere (Hamamatsu Photonics, Japan).

3. Results and discussion

3.1 Phase formation

The phase purity of the as-prepared Cs_3MnBr_5 powder was investigated by the X-ray powder diffraction (XRD) measurement. Profile fitting *via* the Rietveld method was carried out for Cs_3MnBr_5 (Fig. 1a) using TOPAS 4.2.[21] All peaks were indexed by tetragonal unit cell with parameters highly consistent with the reported pattern of Cs_3MnBr_5 (PDF card no. 71-1416). Therefore, this structure was taken as a starting model for the Rietveld refinement. The refinement result shows that this phase has a

tetragonal unit cell of $a = b = 9.60672\ (13)$ Å, $c = 15.5716\ (2)$ Å, and $V = 1437.08\ (4)$ Å^3. Refinement was stable and gave low R-factors, and the detailed information of the refinement processing is provided in Tables S1–S3 in the ESI.† The as-prepared Cs_3MnBr_5 belongs to the tetragonal system under the space group of $14/mcm$, isostructural with Cs_3CoCl_5. In this structure, Mn^{2+} (4b) site is bonded to four bromine atoms, forming a $[MnBr_4]$ regular tetrahedron geometry with D_{2d} symmetry. Cs2 (4a) sites coordinate with ten bromine atoms forming a distorted $[CsBr_{10}]$ polyhedrons, which share two Br1 anions with $[MnBr_4]$ tetrahedrons resulting in an independent distribution of $[MnBr_4]$ tetrahedrons (Fig. 1b). The Cs1 (8h) sites coordinate with eight bromine atoms forming distorted $[CsBr_8]$ polyhedrons, which are linked with each other by faces and form a –$[CsBr_8]$–$[CsBr_8]$– layer. $[MnBr_4]$ tetrahedrons share two Br1 anions with $[CsBr_8]$ polyhedrons forming an alternative layer structure. Moreover, $[MnBr_4]$ in Cs_3MnBr_5 are layer distributed along the c-axis direction, which are separated by $[CsBr_8]$, furthermore, the distance between two neighbouring $[MnBr_4]$ is about 7.785 (6) Å. Inside the ab plane, the distance between two nearest manganese bromide tetrahedrons is approximately 6.785(5) Å (Fig. 1c). And thus, the layer isolation of the sites available for Mn^{2+} leads to the dimensional restriction of energy migration inside the crystal lattices and eventually eliminates the quenching, as discussed below.[22]

To investigate the thermal stability of Cs_3MnBr_5, thermogravimetric analysis (TGA) was carried out from room temperature to 923 K and the mass-change curve is shown in Fig. S1 (ESI†). The sample exhibits good thermal stability up to T = 723 K. The decomposition of the sample is mainly divided into two steps. In the first stage (298–423 K), the mass loss of Cs_3MnBr_5 was 3.76% due to the evaporation of crystal water. The second stage (728–923 K) was the process where the metal(II) bromide decomposed continuously.

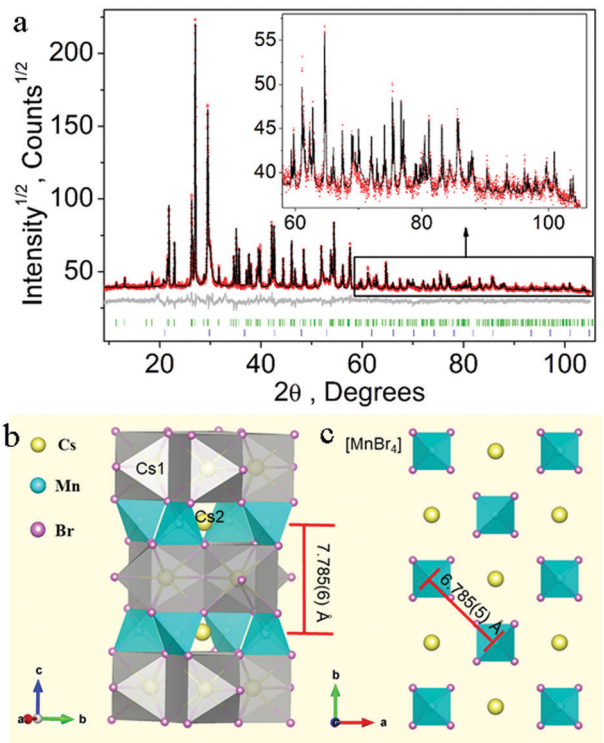

Fig. 1 (a) The Rietveld refinement XRD patterns of Cs_3MnBr_5. (b) Crystal structure of Cs_3MnBr_5. (c) Inside the ab plane, the distance between two nearest manganese bromide tetrahedrons.

The PLE and PL spectra of the Cs_3MnBr_5 phosphor with intrinsic Mn^{2+} emission are shown in Fig. 2a. The excitation spectrum exhibits structured bands with three maxima at 278, 365, and 460 nm because of the energy splitting in the $^4T_1$ excited state with D_{2d} symmetry (Fig. 2a). The intense band centred at 278 nm together with two main absorption peaks at 350 and 460 nm indicate that Cs_3MnBr_5 phosphor can be excited by UV and blue LED chips. Under the excitation at 460 nm, Cs_3MnBr_5 shows a prominent green emission at 520 nm with a FWHM of 42 nm and a high PLQY of 49%. The as-prepared powder also exhibits an intense green light under 365 nm lamp irradiation, as shown in the inset (Fig. 2a). The strong green emission is ascribed to the metal-centred d–d transition of the Mn^{2+} ion in d^5 configuration with a tetrahedral coordination geometry.[23] The detailed energy absorption, non-radiative relaxation and emission process of Mn^{2+} in a tetrahedral environment are described in Fig. 2b. The decay curve of the Cs_3MnBr_5 phosphor under an excitation of 460 nm, monitored at 520 nm at room temperature is presented in Fig. 2c. The decay curve can be fitted using a single exponential decay formula:[24]

$$I(t) = I_0 + A\exp\left(\frac{-t}{\tau}\right) \quad (1)$$

where $I(t)$ and I_0 are the luminescence intensites at time t and $t \gg \tau$, respectively, A is a constant, and τ is the decay time for the exponential component. As shown in Fig. 2c, by using the above fitting equation, the fluorescence lifetime for Cs_3MnBr_5 is determined to be 0.29 ms. The single exponential decay behaviour also confirms the unique Mn^{2+} site in the Cs_3MnBr_5 phosphor.

To prove the potential applications of Cs_3MnBr_5, the β-SiAlON:Eu^{2+} green phosphor was chosen as a reference to compare the optical performance. The dashed dotted red lines in Fig. 2a show the PLE and PL spectra of β-SiAlON:Eu^{2+}, which can be excited by UV to blue light and shows a narrow-band emission at 540 nm with FWHM of 54 nm under 460 nm excitation.[7] Obviously, the PL spectrum of Cs_3MnBr_5 is narrower than that of β-SiAlON:Eu^{2+} with a more proper emission peak (520 nm) for LCD applications, suggesting that Cs_3MnBr_5 is more suitable for wide color gamut display backlights.

Generally, a narrower FWHM implies higher color purity (CP). Therefore, the comparison of CP between Cs_3MnBr_5 and the commercial β-SiAlON:Eu^{2+} phosphors were also studied. The CIE coordinates of the Cs_3MnBr_5 and β-SiAlON:Eu^{2+} phosphors are calculated to be (0.1490, 0.7564) and (0.2405, 0.6312), respectively. The CIE diagram is encircled by monochromatic color coordinates from 380 to 700 nm. The color purity of a specific color is defined by the percentage of the linear distance

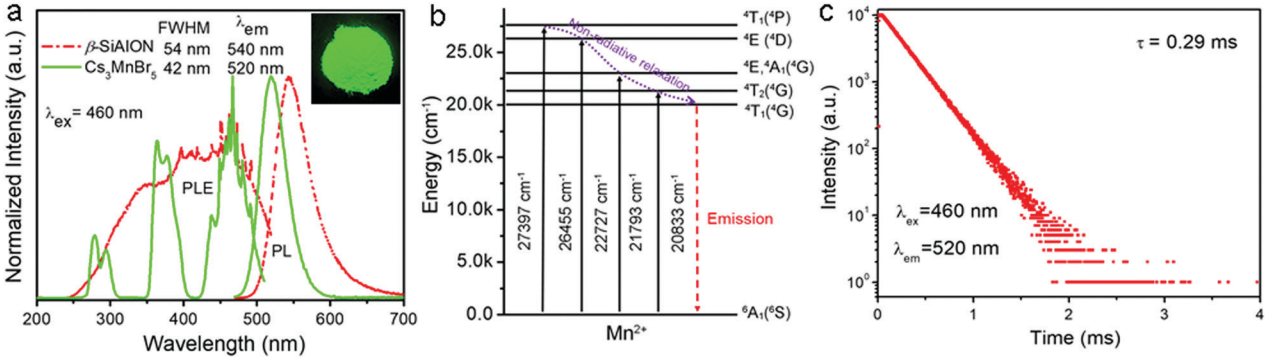

Fig. 2 (a) PLE and PL spectra of Cs_3MnBr_5 (green solid line) and β-SiAlON (red dotted line). The inset shows the digital photographs of green Cs_3MnBr_5 phosphor under 365 nm UV lamp. (b) The decay curve of Cs_3MnBr_5 under excitation at 460 nm, monitored at 520 nm. (c) The schematic diagram showing the energy adsorption, non-radiative relaxation and emission process of Mn^{2+} in a tetrahedral environment.

between the chromaticity coordinates of the sample emission and the CIE1931 standard source to the linear distance between the chromaticity coordinates of the monochromatic light source and the standard source, which can be calculated by the following equation:[25]

$$\text{color purity} = \frac{\sqrt{(x-x_i)^2+(y-y_i)^2}}{\sqrt{(x_d-x_i)^2+(y_d-y_i)^2}} \times 100\% \qquad (2)$$

where (x, y) represents the CIE color coordinates of the Cs_3MnBr_5 and β-SiAlON:Eu^{2+} phosphors, (x_i, y_i) stand for the CIE1931 standard source with CIE color coordinate (0.3333, 0.3333), and (x_d, y_d) is the color coordinate corresponding to the monochromatic light source. The CP of the Cs_3MnBr_5 and β-SiAlON:Eu^{2+} phosphors were calculated to be 78.98% and 59.12%, respectively. The higher CP of the Cs_3MnBr_5 phosphor will help to achieve larger color gamut for backlighting LED. In addition, for phosphors applied to LCD displays, a long decay time will generate ghost signals, which will severely affect the visual effect while watching high definition programs.[13] The comparison of the fluorescence lifetime among the well-known green phosphors is listed in Table 1. The microsecond range of fluorescence lifetime (0.29 ms) of Mn^{2+} in Cs_3MnBr_5 is more shorter than those of Mn^{2+}-doped $MgAl_2O_4$:Mn^{2+}, γ-AlON:Mn^{2+},Mg^{2+} and $Sr_2MgAl_{22}O_{36}$:Mn^{2+} green phosphors with 6.51, 3.89 and 4.71 ms, respectively.[15–17] The abnormal character with a short lifetime value should be related to the intrinsic Mn^{2+} emission in Cs_3MnBr_5, and also to the separation of the $[MnBr_4]$ tetrahedrons from each other. Moreover, the fluorescence lifetimes of Mn^{2+} has only two orders of magnitude difference from that of the Eu^{2+}-doped green phosphors. In other words, the transition metal Mn^{2+}-doped green phosphors with short fluorescence lifetime is expected to achieve more broader applications in backlighting LEDs.

Table 1 The comparisons of fluorescence lifetime of green phosphors and luminous efficiency of WLED devices

Green phosphors	Lifetime	Luminous efficiency (with KSF:Mn^{2+}) (lm W^{-1})	Ref.
β-SiAlON:Eu^{2+}	1 μs	136	7
RLSO:Eu^{2+}	0.84 μs	97.28	13
γ-AlON:Mn^{2+},Mg^{2+}	3.89 ms	—	15
$MgAl_2O_4$:Mn^{2+}	6.51 ms	56.32	23
$Sr_2MgAl_{22}O_{36}$:Mn^{2+}	4.71 ms	70.58	17
Cs_3MnBr_5	0.29 ms	108.8	This work
$Cs_3Mn_{0.96}Zn_{0.04}Br_5$	0.30 ms	107.76	This work

In order to study the effect of Mn^{2+} concentration on the luminescence properties of Cs_3MnBr_5, Zn^{2+} was introduced into Cs_3MnBr_5 to substitute Mn^{2+} partially. The typical XRD patterns of Cs_3MnBr_5:xZn^{2+} samples with varying Zn^{2+} concentrations are shown in Fig. 3a. The results indicate that all the diffraction peaks of the as-prepared Cs_3MnBr_5:xZn^{2+} ($4 \le x \le 30\%$) samples match well with the standard Cs_3MnBr_5 data (PDF card no. 71-1416) and there are no impurity phases with the increase in the Zn^{2+} concentration (x). Both the slight shift of diffraction peaks (right part of Fig. 3a) and the diminution of cell volume (Fig. 3b) are in good agreement with the fact that the radius of Zn^{2+} is smaller than that of Mn^{2+}. In addition, the decrease in the intensity of the EPR signal of Cs_3MnBr_5 further verifies the successful doping of Zn^{2+} ion (Fig. 3c). The PLE and PL spectra of the Cs_3MnBr_5:xZn^{2+} ($4 \le x \le 30\%$) samples are shown in Fig. 3d and e. The PL intensity gradually decreases with the increase in the Zn^{2+} concentration. In addition, both the position and FWHM of the emission band almost remain unchanged (Fig. 3f), which indicates that there is no concentration quenching in the Mn^{2+}-based Cs_3MnBr_5 phosphor. As mentioned above, in Cs_3MnBr_5, the shortest distance between two cesium bromide polyhedrons are 6.785 (5) Å, and therefore, the inter- and intra-layer far distances of cesium bromide polyhedrons will restrict the direction of energy migration, resulting in the high luminescence efficiency without concentration quenching.[22]

The thermal stability of phosphors has an important effect on various performance parameters of the corresponding device.[13] Thus, temperature is a critical parameter to evaluate the potential application of phosphors. Fig. 4a and b comparatively shows the temperature-dependent PL spectra of Cs_3MnBr_5 and $Cs_3Mn_{0.96}Zn_{0.04}Br_5$ phosphors from room temperature (RT, 298 K) to 523 K with a step interval of 25 K. With the increase in the temperature, the emission intensity gradually decreases, which is caused by the non-radiative transitions due to the lattice vibration

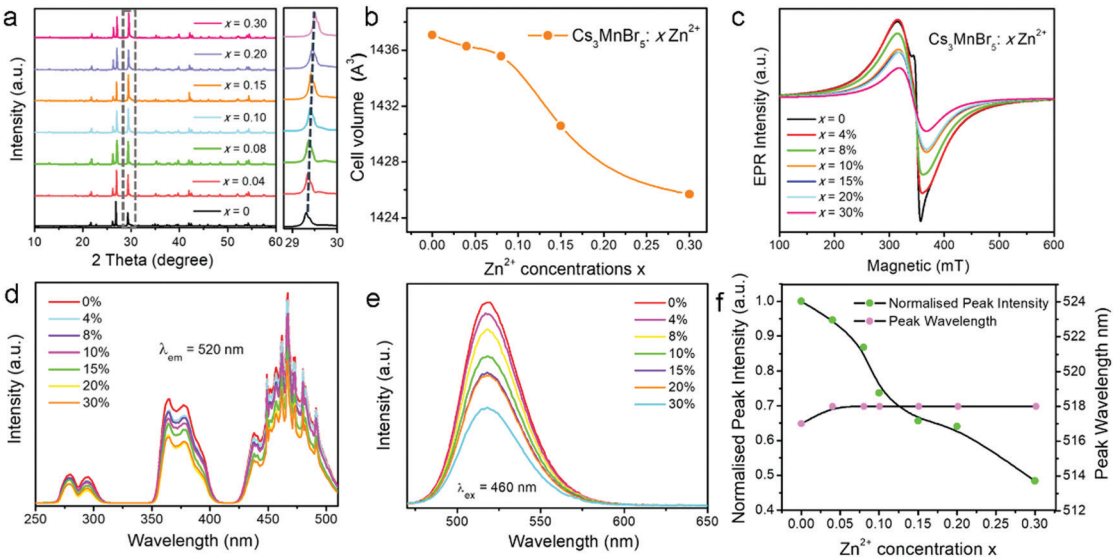

Fig. 3 (a) XRD pattern of $Cs_3Mn_{1-x}Br_5$:xZn^{2+} (x = 0–0.30). (b) The variation of cell volume of Cs_3MnBr_5:xZn^{2+} (x = 0.04, 0.08, 0.15, 0.30). (c) EPR spectra of Zn^{2+}-doped Cs_3MnBr_5 obtained with different Zn^{2+} : Mn^{2+} ratios. The PLE (d) and PL (e) spectra of Cs_3MnBr_5:xZn^{2+} (x = 4%, 8%, 10%, 15%, 20%, 30%). (f) The intensity and wavelength change of emission peak for different doping concentrations of Zn^{2+}.

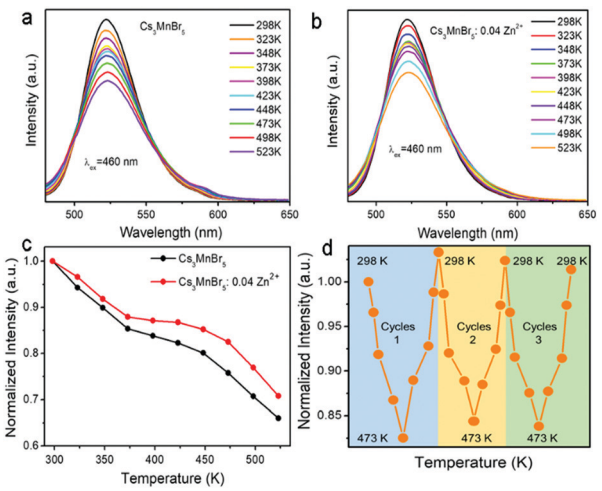

Fig. 4 Temperature-dependent PL spectra of Cs_3MnBr_5 (a) and $Cs_3Mn_{0.96}Zn_{0.04}Br_5$ (b) under 460 nm excitation in the temperature range of RT-523 K with a temperature interval of 298 K. (c) Temperature-dependent normalized integrated PL intensities of Cs_3MnBr_5 and $Cs_3Mn_{0.96}Zn_{0.04}Br_5$. (d) The corresponding emission intensity with three heating and cooling cycles of the $Cs_3Mn_{0.96}Zn_{0.04}Br_5$ phosphor from 298 to 473 K.

and the lattice relaxation of the luminescent centres.[15] The comparison of integrated PL intensities between Cs_3MnBr_5 and $Cs_3Mn_{0.96}Zn_{0.04}Br_5$ from 298 to 523 K is shown in Fig. 4c. The Cs_3MnBr_5 presents a relatively low luminescence quenching behaviour even at 423 K with an integrated PL intensity around 82% of the initial intensity measured at 298 K. Moreover, integrated PL intensities of $Cs_3Mn_{0.96}Zn_{0.04}Br_5$ still remain 87% at 423 K, which indicates that the doping of Zn^{2+} into Cs_3MnBr_5 effectively improves the thermal stability. The trends of integrated PL intensities with three heating and cooling cycles of the $Cs_3Mn_{0.96}Zn_{0.04}Br_5$ from 298 to 473 K also have been investigated and are shown in Fig. 4d. After three cycles of heating and cooling process, the thermal stability of $Cs_3Mn_{0.96}Zn_{0.04}Br_5$ almost remain unchanged and the integrated PL intensity even has a slight promotion after cooling to room temperature. All of these results indicate that $Cs_3Mn_{0.96}Zn_{0.04}Br_5$ phosphor possesses better temperature-dependent stability and can hence play a key role in the green phosphors used in backlighting displays.

Considering the practicability of synthesized phosphors in wide color gamut display backlights, the LEDs integrated with green phosphor Cs_3MnBr_5 or $Cs_3Mn_{0.96}Zn_{0.04}Br_5$, red phosphor K_2SiF_6:Mn^{4+}, and commercial blue emitting InGaN chips were fabricated, which are denoted as LED-1 (Cs_3MnBr_5) and LED-2 ($Cs_3Mn_{0.96}Zn_{0.04}Br_5$). The PL spectra of the fabricated LED devices under a current of 20 mA are shown in Fig. 5a and b; the inset shows the photographs of the LED devices. The LED-1 and LED-2 show a bright white light with a high luminous efficiency up to 108.88 lm W^{-1} and 107.76 lm W^{-1}, respectively, which are higher than other previously reported phosphor-converted WLEDs (Table 1), except for the recently reported β-SiAlON:Eu^{2+} based WLED. The calculated color gamut covers the color space of 104% and 101% in CIE 1931 with CIE color coordinates (0.3098, 0.3226) and (0.2989, 0.3042), respectively. Fig. 5d and e show the PL spectra of the fabricated LEDs under the various operating currents. Compared with LED-1, LED-2 exhibits better stability and the PL intensity of $Cs_3Mn_{0.96}Zn_{0.04}Br_5$ still remains 86% at 140 mA operating current (Fig. 5f). The results demonstrate that the introduction of Zn^{2+} into Cs_3MnBr_5 significantly improved the stability of the LED device. $Cs_3Mn_{0.96}Zn_{0.04}Br_5$ can thus be utilized for broad potential applications in LCD backlight displays.

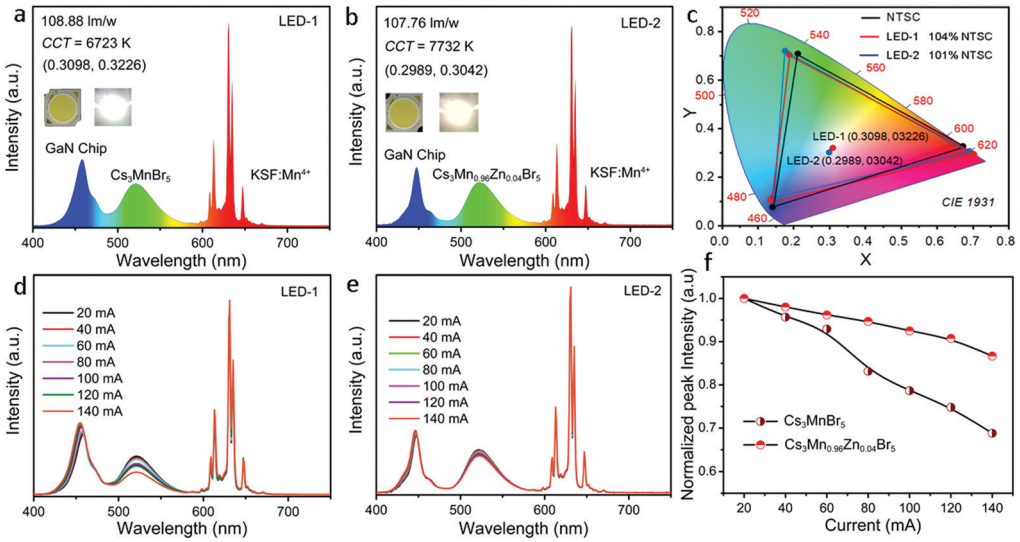

Fig. 5 (a and b) PL spectrum of the WLED devices fabricated with the green phosphor Cs_3MnBr_5, $Cs_3Mn_{0.96}Zn_{0.04}Br_5$ and the commercial red phosphor KSF:Mn^{4+} on a blue LED GaN chip under a current of 20 mA respectively. The inset shows the photographs of the as-fabricated and lightened LEDs. (c) CIE 1931 color coordinates of fabricated LEDs, and color space of NTSC standard (red line) and LED-1 (black line) and LED-2 (blue line). (d and e) PL spectra of the fabricated LEDs under various operating currents. (f) The peak intensity variation of green phosphors in WLEDs under various operating currents.

4. Conclusions

In summary, we have synthesized a novel Mn^{2+}-based narrow-band green-emitting Cs_3MnBr_5 phosphor with λ_{em} = 520 nm, FWHM = 42 nm and the luminescence originates from the intrinsic Mn^{2+} d–d transition with abnormal short fluorescence lifetime value originating from the separated [$MnBr_4$] tetrahedrons without concentration quenching. The thermal stability of Cs_3MnBr_5 was improved from 82% to 87% at 423 K by introducing a small amount of Zn^{2+} into Cs_3MnBr_5. By combining $Cs_3Mn_{0.96}Zn_{0.04}Br_5$ green phosphor, KSF:Mn^{4+} red phosphor and blue InGaN chips, the fabricated LED device shows a high luminous efficiency up to 107.66 lm W^{-1} with a wide color gamut of 101% NTSC for backlight display, which is larger than that of white LED based on commercial green phosphor β-SiAlON:Eu^{2+} (89%). All results indicate that Cs_3MnBr_5 and $Cs_3Mn_{0.96}Zn_{0.04}Br_5$ phosphors can act as promising narrow-band emitting green phosphors in the field of wide-color-gamut LCD backlight displays.

Conflicts of interest

The authors declare no conflicts of interest.

Acknowledgements

The present work was supported by the National Natural Science Foundations of China (Grant No. 51722202, 51972118 and 51572023), Natural Science Foundations of Beijing (2172036) and the Guangdong Provincial Science & Technology Project (no. 2018A050506004).

References

1 Z. G. Xia and Q. L. Liu, *Prog. Mater. Sci.*, 2016, **84**, 59–117.
2 J. Zhou, Q. L. Liu and Z. G. Xia, *J. Mater. Chem. C*, 2018, **6**, 4371–4383.
3 P. Pust, V. Weiler, C. Hecht, A. Tucks, A. S. Wochnik, A. K. Henss, D. Wiechert, C. Scheu, P. J. Schmidt and W. Schnick, *Nat. Mater.*, 2014, **13**, 891–896.
4 L. Wang, X. Wang, T. Kohsei, K. Yoshimura, M. Izumi, N. Hirosaki and R. J. Xie, *Opt. Express*, 2015, **23**, 28707–28717.
5 P. Pust, P. J. Schmidt and W. Schnick, *Nat. Mater.*, 2015, **14**, 454–458.
6 N. Hirosaki, R. J. Xie, K. Kimoto, T. Sekiguchi, Y. Yamamoto, T. Suehiro and M. Mitomo, *Appl. Phys. Lett.*, 2005, **86**, 211905.
7 S. Li, L. Wang, D. Tang, Y. Cho, X. Liu, X. Zhou, L. Lu, L. Zhang, T. Takeda, N. Hirosaki and R. J. Xie, *Chem. Mater.*, 2017, **30**, 494–505.
8 X. J. Zhang, H. C. Wang, A. C. Tang, S. Y. Lin, H. C. Tong, C. Y. Chen, Y. C. Lee, T. L. Tsai and R. S. Liu, *Chem. Mater.*, 2016, **28**, 8493–8497.
9 H. Wu, Y. Yang, D. C. Zhou, K. R. Li, J. Yu, J. Han, Z. C. Li, Z. W. Long, J. Ma and J. B. Qiu, *Nanoscale*, 2018, **10**, 3429–3437.
10 P. Strobel, S. Schmiechen, M. Siegert, A. Tücks, P. J. Schmidt and W. Schnick, *Chem. Mater.*, 2015, **27**, 6109–6115.
11 T. Takeda, N. Hirosaki, S. Funahshi and R. J. Xie, *Chem. Mater.*, 2015, **27**, 5892–5898.
12 M. Zhao, H. X. Liao, L. X. Ning, Q. Y. Zhang, Q. L. Liu and Z. G. Xia, *Adv. Mater.*, 2018, **30**, 1802489.
13 H. X. Liao, M. Zhao, Y. Y. Zhou, M. S. Molokeev, Q. L. Liu, Q. Y. Zhang and Z. G. Xia, *Adv. Funct. Mater.*, 2019, 201901988.

14 Z. W. Long, Y. G. Wen, J. B. Qiu, J. Wang, D. C. Zhou, C. C. Zhu, J. A. Lai, X. H. Xu, X. Yu and Q. Wang, *Chem. Eng. J.*, 2019, **375**, 122016.
15 Y. L. Zhu, Y. J. Liang, S. Q. Liu, H. R. Li and J. H. Chen, *Adv. Opt. Mater.*, 2019, **7**, 1801419.
16 E. H. Song, Y. Y. Zhou, Y. Wei, X. X. Han, Z. R. Tao, R. L. Qiu, Z. G. Xia and Q. Y. Zhang, *J. Mater. Chem. C*, 2019, **7**, 8192–8198.
17 Q. Dong, F. L. Yang, J. Cui, Y. B. Tian, S. F. Liu, F. Du, J. Q. Peng and X. Y. Ye, *Ceram. Int.*, 2019, **45**, 11868–11875.
18 S. Zhang, H. B. Liang, Y. W. Liu, Y. F. Liu, D. J. Hou, G. B. Zhang and J. Y. Shi, *Opt. Lett.*, 2012, **37**, 2511–2513.
19 Z. C. Li, L. Kong, S. Q. Huang and L. Li, *Angew. Chem., Int. Ed.*, 2017, **56**, 8134–8138.
20 H. C. Wang, S. Y. Lin, A. C. Tang, B. P. Singh, H. C. Tong, C. Y. Chen, Y. C. Lee, T. L. Tsai and R. S. Liu, *Angew. Chem., Int. Ed.*, 2016, **55**, 7924–7929.
21 V. Topas, Bruker AXS, Karlsruhe, Germany, 2008.
22 J. H. Li, Q. Y. Liang, Y. F. Cao, J. Yan, J. B. Zhou, Y. Q. Xu, L. Dolgov, Y. Y. Meng, J. X. Shi and M. M. Wu, *ACS Appl. Mater. Interfaces*, 2018, **10**, 41479–41486.
23 D. Palumbo and J. Brown, *J. Electrochem. Soc.*, 1970, **117**, 1184–1188.
24 G. Blasse and B. C. Grabmaier, *Luminescent Materials*, Springer, Berlin, 1994.
25 U. Caldiño, A. Lira, A. N. Meza Rocha, I. Camarillo and R. Lozada Morales, *J. Lumin.*, 2018, **194**, 231–239.